Impermeability effects in three-dimensional vesicles

2004 J. Phys. A: Math. Gen. 37 6859

(http://iopscience.iop.org/0305-4470/37/27/001)

INSTITUTE OF PHYSICS PUBLISHING JOURNAL OF PHYSICS A: MATHEMATICAL AND GENERAL

J. Phys. A: Math. Gen. **37** (2004) 6859–6874 PII: S0305-4470(04)73558-1

Impermeability effects in three-dimensional vesicles

P Biscari[1,2], **S M Canevese**[3] **and G Napoli**[1]

[1] Dipartimento di Matematica, Politecnico di Milano, Piazza Leonardo da Vinci 32-20133 Milano, Italy
[2] Istituto Nazionale di Fisica della Materia, Via Ferrata 1-27100 Pavia, Italy
[3] Dipartimento di Elettronica e Informazione, Politecnico di Milano, Via Ponzio 34-20133 Milano, Italy

E-mail: paoleo.biscari@polimi.it, canevese@elet.polimi.it and gaetano.napoli@mate.polimi.it

Received 16 December 2003
Published 22 June 2004
Online at stacks.iop.org/JPhysA/37/6859
doi:10.1088/0305-4470/37/27/001

Abstract

We analyse the effects of the impermeability constraint on the equilibrium shapes of a three-dimensional vesicle hosting a rigid inclusion. A given alteration of the inclusion and/or vesicle parameters leads to shape modifications of different orders of magnitude, when applied to permeable or impermeable vesicles. Moreover, the enclosed-volume constraint wrecks the uniqueness of stationary equilibrium shapes, and gives rise to pear-shaped or stomatocyte-like vesicles.

PACS numbers: 87.16.Dg, 87.15.He
Mathematics Subject Classification: 74L15, 74K15, 74B15

1. Introduction

Proteins embedded in biological membranes strongly influence both the geometric and the elastic properties of the hosting membranes. The rigid inclusions are able to induce vesicle budding [1–3], while the interplay between the protein–membrane interaction and the spontaneous curvature may yield a loss of regular equilibrium configurations [4]. Moreover, the elasticity of the hosting vesicle induces a membrane-mediated interaction that has been widely studied both experimentally [5] and theoretically, in the cases of planar [6, 7], quasi-planar [8–10] and quasi-spherical vesicles [11].

In this paper we focus our attention on the equilibrium shapes of a three-dimensional vesicle hosting a rigid inclusion, and in particular on the effects of the permeability properties of the vesicle. In fact, a given slight perturbation applied to a quasi-spherical vesicle may induce quite different changes on the resulting equilibrium shape, depending on whether the enclosed volume of the vesicle is constrained or not. More precisely, an $O(\epsilon)$ relative perturbation of the external parameters induces an equivalent $O(\epsilon)$ modification in the shape

function of a permeable vesicle, but a stronger $O(\sqrt{\epsilon})$ relative perturbation if the enclosed volume is kept fixed. Furthermore, the volume constraint yields a multiplicity of stationary equilibrium shapes, and it leads to the abandonment of the spherical shape towards either pear-shaped or stomatocyte-like vesicles.

Whether the volume enclosed by the vesicle may be constrained or not depending on both the chemical properties of the aqueous solution which surrounds the vesicle, and the time scales on which the (meta)equilibrium shapes are observed [12, 13]. When the water is essentially free of molecules that cannot permeate the bilayer membrane, no volume constraint stands. In contrast, when some of the molecules in the solution are unable to permeate the bilayer, the resulting osmotic pressure gives rise to an enclosed-volume constraint. However, even in this latter case, on long time scales water molecules succeed in permeating the membrane. Eventually, the vesicle reaches its true equilibrium shape, which minimizes the free energy with respect to the enclosed volume.

Throughout our development, we will model proteins as rigid inclusions, and we will assume that the protein–membrane interaction simply fixes the contact angle, i.e. the angle the vesicle normal determines with the inclusion plane [14, 8, 15]. However, only small modifications need to be applied to our results to take into account interactions which determine the contact curvature instead of the contact angle [16–18]. More drastic changes, though substantially the same mathematical setting, require the weak anchoring case [15, 19, 4], in which the inclusion–vesicle interaction provides an additional term in the free-energy functional, instead of a fixed boundary condition.

We describe vesicle elasticity through Helfrich's (spontaneous curvature) model [20, 21]. The free-energy functional is then

$$\mathcal{F}[\Sigma] := \kappa \int_{\Sigma} (H - \sigma_0)^2 \, \mathrm{d}a \tag{1.1}$$

where Σ is a closed surface describing the vesicle shape, H denotes the mean curvature along Σ, κ is the bending energy and σ_0 the spontaneous curvature. In the minimizing procedure at fixed area (and possibly fixed volume) we replace (1.1) with the effective free-energy functional

$$\mathcal{F}_{\mathrm{eff}}[\Sigma] := \kappa \int_{\Sigma} (H - \sigma_0)^2 \, \mathrm{d}a + \lambda(\mathrm{Area}(\Sigma) - A) + [\![\mu(\mathrm{Vol}(\Sigma) - V)]\!]. \tag{1.2}$$

The Lagrange multipliers λ and μ have the physical meaning of surface tension and pressure difference and the brackets are there to remind us that the volume constraint will not always be applied. In (1.2) the area constraint has been inserted as a global, instead of a local constraint. We recall that, in the absence of external forces, both choices are equivalent [22].

The Euler–Lagrange equation associated with the functional (1.2) is the *shape equation* [22, 23]:

$$\kappa\left[\Delta_{\mathrm{s}} H + 2H(H^2 - K) + 2\sigma_0 K - 2\sigma_0^2 H\right] - 2\lambda H - [\![\mu]\!] = 0 \tag{1.3}$$

where Δ_{s}, the tangential divergence of the tangential gradient, is the Laplace–Beltrami operator on Σ and K denotes the Gaussian curvature along Σ.

The plan of the paper is as follows. In the next section, we introduce the surface parametrization and we derive the conditions satisfied by spherical and quasi-spherical shapes. In section 3 we analyse the vesicle shapes obtained in the presence of the area constraint alone (i.e. the long-time equilibrium vesicle shapes). Section 4 is devoted to the peculiar role played by the volume constraint. In section 5 we review and discuss our results.

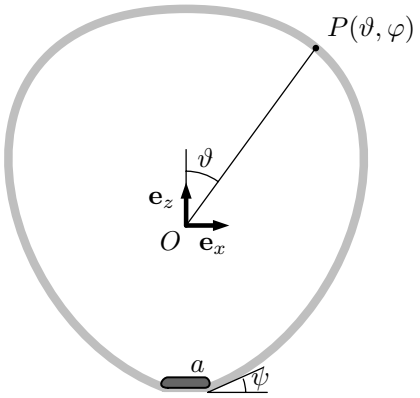

Figure 1. Cross-section of a three-dimensional vesicle embedding a conical inclusion of base radius a. The tangent to the generating curve at the contact points determines a fixed angle ψ with the inclusion plane.

2. The model

Let us consider a vesicle that embeds an inclusion which we model as a symmetric conical frustum of negligible height, base radius a and apex angle ψ. The inclusion–vesicle interaction fixes the angle between the vesicle normal and the inclusion plane at the contact points to be equal to $\left(\frac{\pi}{2}-\psi\right)$. Figure 1 illustrates the geometric setup of the model. For a more detailed description of the inclusion–vesicle interactions and their modelling we refer the reader to the paper by Biscari and Rosso [4].

We restrict our analysis to axisymmetric vesicle shapes and parametrize them in spherical coordinates centred at a fixed point O, which lies in the inclusion symmetry axis z (we assume that this is the symmetry axis of the vesicle too, since the inclusion does not upset the cylindrical symmetry):

$$P(\vartheta,\varphi)-O=r(\vartheta)\sin\vartheta\cos\varphi\,\mathbf{e}_x+r(\vartheta)\sin\vartheta\sin\varphi\,\mathbf{e}_y+r(\vartheta)\cos\vartheta\,\mathbf{e}_z.$$

The unit vectors $\{\mathbf{e}_x,\mathbf{e}_y,\mathbf{e}_z\}$ form an orthogonal basis, with $\mathbf{e}_z$ parallel to the inclusion axis; ϑ and φ are the polar and azimuthal angles, respectively. The area element, the Laplace–Beltrami operator, the mean curvature and the Gaussian curvature along Σ are given by

$$\mathrm{d}a=\sqrt{g}\,\mathrm{d}\vartheta\,\mathrm{d}\varphi\qquad \Delta_{\mathrm{s}}=\frac{1}{\sqrt{g}}\left[\partial_\vartheta\left(\frac{r\sin\vartheta}{\sqrt{r^2+r'^2}}\partial_\vartheta\right)+\partial_\varphi\left(\frac{\sqrt{r^2+r'^2}}{r\sin\vartheta}\partial_\varphi\right)\right]$$

$$H=\frac{2r^3+3rr'^2-r'^3\cot\vartheta-r^2(r'\cot\vartheta+r'')}{2r(r^2+r'^2)^{3/2}}$$

and

$$K=\frac{(r\sin\vartheta-r'\cos\vartheta)(r^2+2r'^2-rr'')}{r\sin\vartheta\,(r^2+r'^2)^2}$$

where a prime denotes differentiation with respect to the polar angle and $g:=(r^2+r'^2)r^2\sin^2\vartheta$. The spherical parametrization transforms the effective free energy (1.2) as follows:

$$\mathcal{F}_{\mathrm{eff}}[r]=2\pi\int_0^{\vartheta_{\mathrm{f}}}(\kappa(H[r]-\sigma_0)^2+\lambda)\,r\sqrt{r^2+r'^2}\sin\vartheta\,\mathrm{d}\vartheta+\left[\!\!\left[\frac{2\pi}{3}\mu\int_0^{\vartheta_{\mathrm{f}}}r^3(\vartheta)\sin\vartheta\,\mathrm{d}\vartheta\right]\!\!\right].$$

The integration limit ϑ_f depends on the position of the origin O. We choose to fix O at a distance $\Delta z = (a \cot \psi)$ above the inclusion, which yields $\vartheta_f = (\pi - \psi)$. This choice simplifies the attachment condition on the inclusion and the constraint on the direction of the contact normal, which become

$$r(\vartheta_f) = \frac{a}{\sin \psi} \qquad \text{and} \qquad r'(\vartheta_f) = 0. \tag{2.1}$$

The vesicle is free on its top ($\vartheta = 0$). The boundary conditions therein follow from regularity requirements on the vesicle shape:

$$\lim_{\vartheta \to 0^+} r'(\vartheta) = 0 \qquad \text{and} \qquad \lim_{\vartheta \to 0^+} r'''(\vartheta) = 0. \tag{2.2}$$

2.1. Internal actions

Let us consider a subsurface $\Sigma' \subseteq \Sigma$, and let $\mathbf{n}$ and $\mathbf{t}$ respectively denote the normal to Σ at a point $P \in \partial\Sigma'$, and the tangent to the curve $\partial\Sigma'$. Furthermore, let $\mathbf{k} := \mathbf{n} \wedge \mathbf{t}$ denote the direction in the tangent plane at P pointing outwards with respect to Σ'. The internal actions at P consist in a distributed force $\mathbf{f}$ and a distributed torque $\mathbf{m}$, whose densities per unit length of $\partial\Sigma'$ are

$$\mathbf{f} = [\kappa(H - \sigma_0)^2 + \lambda]\,\mathbf{k} - \kappa \frac{\partial H}{\partial k}\mathbf{n} \qquad \text{and} \qquad \mathbf{m} = \kappa(H - \sigma_0)\mathbf{n}.$$

The above equations generalize to three-dimensional vesicles the internal actions derived in [7] for the two-dimensional case. They show that the surface tension λ may become negative without giving rise to the collapse of the vesicle, provided that $\mathbf{f} \cdot \mathbf{k} = [\kappa(H - \sigma_0)^2 + \lambda]$ remains non-negative all along the vesicle. Furthermore, they provide an alternative way of deriving the free-boundary conditions (2.2). In fact, these conditions are equivalent to the vanishing of the internal force and torque acting on an infinitesimal cap which surrounds the vesicle top.

2.2. Spherical shapes

The equilibrium shape of a vesicle is a sphere of radius r_0, centred at O, whenever the base radius a_0, the apex angle ψ_0 and the vesicle area A_0 satisfy

$$a_0 = r_0 \sin \psi_0 \qquad \text{and} \qquad A_0 = 4\pi r_0^2 \cos^2 \frac{\psi_0}{2}. \tag{2.3}$$

If we eliminate r_0 from equations $(2.3)_1$ and $(2.3)_2$, we obtain

$$\pi a_0^2 = A_0 \sin^2 \frac{\psi_0}{2}.$$

If, in addition, the vesicle is impermeable, the enclosed volume V_0 must match

$$V_0 = \frac{4}{3}\pi r_0^3 \cos^2 \frac{\psi_0}{2} + \frac{1}{3}\pi a_0^2 r_0 \cos \psi_0 = \frac{\pi a_0^3}{6} \frac{\cos \frac{\psi_0}{2}}{\sin^3 \frac{\psi_0}{2}} (2 - \cos \psi_0).$$

In particular, the area, enclosed volume and the apex angle must obey

$$\upsilon_0 := 36\pi \frac{V_0^2}{A_0^3} = (2 - \cos \psi_0)^2 \cos^2 \frac{\psi_0}{2}. \tag{2.4}$$

We remark that for any value in $\upsilon_0 \in [1, 2]$ (the end cases corresponding to the cases of a sphere and a half sphere), there is exactly one value of $\psi_0 \in \left[0, \frac{\pi}{2}\right]$ that satisfies (2.4).

2.3. Quasi-spherical shapes

We now assume that some of the control parameters a, ψ, A (and possibly V) are slightly perturbed with respect to their values satisfying (2.3) and (2.4). In this case, we look for solutions of the shape equation (1.3) that represent a perturbation of a sphere:

$$r(\vartheta) = r_0(1 + \epsilon\varrho_1(\vartheta) + o(\epsilon)). \tag{2.5}$$

Consistently, we also expand the Lagrange multipliers by perturbing their 'spherical' values

$$\lambda = \frac{\kappa}{r_0^2}(\Lambda_0 + \epsilon\Lambda_1 + o(\epsilon)) \qquad \text{and} \qquad \mu = \frac{2\kappa}{r_0^3}(\eta_0 + \epsilon\eta_1 + o(\epsilon)). \tag{2.6}$$

In (2.6), the normalizing factors κ and r_0 have been inserted in order to proceed with the dimensionless quantities Λ_i and η_i. Furthermore, in order to make the whole shape equation dimensionless, we define the reduced spontaneous curvature as

$$\varsigma_0 := \sigma_0 r_0. \tag{2.7}$$

If we insert (2.5), (2.6) and (2.7) in (1.3), we derive for $O(1)$ the condition

$$\Lambda_0 + \eta_0 = \varsigma_0(1 - \varsigma_0) \tag{2.8}$$

linking the spherical values of the Lagrange multipliers.

When we push the expansion to $O(\epsilon)$, we obtain a fourth-order linear differential equation for ϱ_1. If we further introduce the variable $s := \cos\vartheta$, and perform the substitution $\varrho_1(\vartheta) = \varpi_1(\cos\vartheta)$, the so-obtained differential equation reads

$$\begin{aligned}(1-s^2)^2\varpi^{(4)} - 8s(1-s^2)\varpi^{(3)} + [12s^2 - 4 + g_1(1-s^2)]\varpi^{(2)} - 2g_1 s\varpi^{(1)} + g_0\varpi \\ = -4(\Lambda_1 + \eta_1)\end{aligned} \tag{2.9}$$

where

$$g_0 = 2g_1 := 4(\varsigma_0(2 - \varsigma_0) - \Lambda_0)$$

and the superscripts denote differentiation with respect to s. Equation (2.9) is an inhomogeneous fourth-order Legendre differential equation. Its general solution can be expressed in terms of Legendre functions of the first and second kind as

$$\varpi(s) = -\frac{4(\Lambda_1 + \eta_1)}{g_0} + C_1 P_{\nu_+}(s) + C_2 Q_{\nu_+}(s) + C_3 P_{\nu_-}(s) + C_4 Q_{\nu_-}(s)$$

where the orders of the Legendre functions are given by

$$\nu_\pm = -\tfrac{1}{2} + \tfrac{1}{2}\sqrt{5 + 2g_1 \pm 2\sqrt{(g_1+2)^2 - 4g_0}}. \tag{2.10}$$

If we replace $g_0 = 2g_1$ in (2.10), we obtain $\nu_\pm = -\frac{1}{2} + \frac{1}{2}\sqrt{5 + 2g_1 \pm 2\,|g_1 - 2|}$, so that

$$\{\nu_+, \nu_-\} = \left\{1, \tfrac{1}{2}\left(\sqrt{1 + 4g_1} - 1\right)\right\}.$$

If we further introduce the notation

$$\nu := \tfrac{1}{2}\left(\sqrt{1 + 4g_1} - 1\right) = \tfrac{1}{2}\left(\sqrt{1 + 8\varsigma_0(2 - \varsigma_0) - 8\Lambda_0} - 1\right) \tag{2.11}$$

and we finally consider that $P_1(s) = s$, we arrive at the general solution of the linearized shape equation

$$\varrho_1(\vartheta) = -\frac{4(\Lambda_1 + \eta_1)}{g_0} + C_1\cos\vartheta + C_2 Q_1(\cos\vartheta) + C_3 P_\nu(\cos\vartheta) + C_4 Q_\nu(\cos\vartheta). \tag{2.12}$$

Some further investigation will turn out to be necessary in the particular cases $\nu = 0$ (i.e. $g_1 = 0$) and $\nu = 1$ (i.e. $g_1 = 2$). We postpone the analysis of these cases to the sections below.

In the following, we will analyse and compare the perturbed equilibrium vesicle shapes of permeable and impermeable vesicles. The derivation below works when any or even all of the parameters a, ψ, A or V are varied with respect to their spherical values. However, and only in order to shorten our presentation, we will henceforth restrict our development to the case in which only the area, and possibly the enclosed volume, are varied with respect to the values satisfying (2.3) and (2.4), while the inclusion parameters are kept unchanged. These are the easiest perturbations to implement experimentally: for example, an area variation in a biological membrane may be simply induced by adding extra lipid molecules to the membrane bilayer.

3. Permeable vesicles

When the vesicle is inextensible but permeable, no volume constraint stands. For all practical purposes, this is equivalent to assuming that the Lagrange multiplier μ vanishes identically. When this is the case, condition (2.8) reads

$$\Lambda_0 = \varsigma_0(1 - \varsigma_0)$$

which implies $g_0 = 2g_1 = 4\varsigma_0$ and

$$\nu = \tfrac{1}{2}\big(\sqrt{1 + 8\varsigma_0} - 1\big). \tag{3.1}$$

The linear perturbation of the spherical shape becomes

$$\varrho_1(\vartheta) = -\frac{\Lambda_1}{\varsigma_0} + C_1 \cos\vartheta + C_2 Q_1(\cos\vartheta) + C_3 P_\nu(\cos\vartheta) + C_4 Q_\nu(\cos\vartheta). \tag{3.2}$$

All Legendre functions of the second kind $Q_\nu(s)$ are singular when $s \to 1^-$. Thus, the free-boundary conditions (2.2) require $C_2 = C_4 = 0$. The remaining parameters Λ_1, C_1 and C_3 can be determined with the aid of the contact conditions (2.1) and the area constraint:

$$\varrho_1(\vartheta_\mathrm{f}) = 0 \qquad \varrho_1'(\vartheta_\mathrm{f}) = 0 \qquad \text{and} \qquad 4\pi r_0^2 \int_0^{\vartheta_\mathrm{f}} \varrho_1(\vartheta)\sin\vartheta\,\mathrm{d}\vartheta = \Delta A \tag{3.3}$$

where ΔA is the excess area with respect to the spherical value A_0. With the aid of (A.2)–(A.4) conditions (3.3) yield

$$\Lambda_1 = \varsigma_0 C_3 \operatorname{cosec}^2\psi_0[\nu\cos\psi_0 P_{\nu-1}(-\cos\psi_0) + (\sin^2\psi_0 + \nu\cos^2\psi_0)P_\nu(-\cos\psi_0)]$$
$$C_1 = -\nu C_3 \operatorname{cosec}^2\psi_0[P_{\nu-1}(-\cos\psi_0) + \cos\psi_0 P_\nu(-\cos\psi_0)]$$

and

$$\frac{C_3}{(\nu+1)(1-\cos\psi_0)}\left[\frac{4(P_{\nu-1}(-\cos\psi_0) - P_\nu(-\cos\psi_0))}{1+\cos\psi_0} - (\nu-1)(\nu\cos\psi_0 + 2)P_\nu(-\cos\psi_0) - (\nu^2+\nu+2)P_{\nu-1}(-\cos\psi_0)\right] = \frac{\Delta A}{A_0}.$$

We have already announced that the differential equation (2.9) admits (3.2) as its general solution only when $\nu \notin \{0, 1\}$, that is when the spontaneous curvature is neither null nor equal to the inverse of the unperturbed radius r_0. We will now solve (2.9) in these cases.

When $\varsigma_0 = 0$, the general solution of the homogeneous differential equation associated with (2.9) is still as in (3.2), with $\nu = 0$. However, and since $P_0(s) \equiv 1$, the particular solution of the equation is not a constant. By using the method of variation of parameters, and requiring also the free-boundary conditions (2.2), we find

$$\varrho_1^{(\varsigma_0=0)}(\vartheta) = C_1\cos\vartheta + C_3 + \Lambda_1(3 + 2\lg(1+\cos\vartheta)).$$

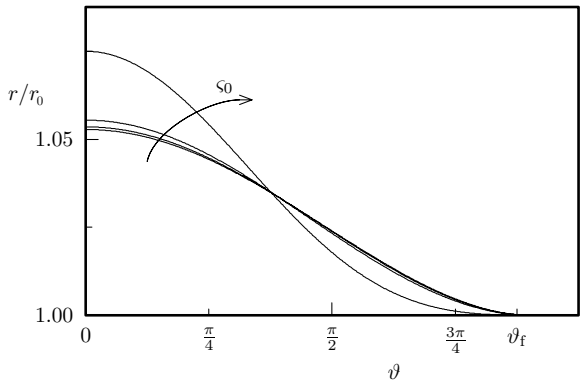

Figure 2. Perturbed shapes of a vesicle hosting an inclusion, when the area is slightly greater than the area corresponding to a spherical equilibrium solution. The plots correspond to $\psi_0 = 0.1\pi$, $\Delta A = 0.05A_0$ and $\varsigma_0 = 0, 1, 2, 3$ (the arrow points towards increasing values of ς_0).

In addition, conditions (3.3) yield

$$\Lambda_1 = -C_1 \sin^2 \frac{\psi_0}{2} \qquad C_3 = C_1 \left[1 + \left(1 + 2 \lg \left(2 \sin^2 \frac{\psi_0}{2} \right) \right) \sin^2 \frac{\psi_0}{2} \right]$$

and

$$2 \left(1 + \sin^2 \frac{\psi_0}{2} + 2 \tan^2 \frac{\psi_0}{2} \lg \sin^2 \frac{\psi_0}{2} \right) C_1 = \frac{\Delta A}{A_0}.$$

When $\varsigma_0 = 1$, the particular solution of the differential equation (2.9) is again a constant, but the solution of the homogeneous equation is not of the form (3.2). If we solve (2.9) explicitly and use the free-boundary conditions (2.2), we arrive at

$$\varrho_1^{(\varsigma_0=1)}(\vartheta) = C_1 \cos\vartheta + C_3(\cos\vartheta \lg(1 + \cos\vartheta) - 1) - \Lambda_1.$$

Finally, conditions (3.3) now require

$$C_1 = -C_3 \left(\lg(1 - \cos\psi_0) - \frac{\cos\psi_0}{1 - \cos\psi_0} \right)$$

$$\Lambda_1 = -C_3 \left(1 + \frac{\cos^2\psi_0}{1 - \cos\psi_0} \right) \qquad \text{and} \qquad \cos^2 \frac{\psi_0}{2} \cot^2 \frac{\psi_0}{2} C_3 = \frac{\Delta A}{A_0}.$$

Figure 2 shows how the perturbed vesicle shape depends on the spontaneous curvature for a prescribed area increase (5% with respect to the spherical value), while figure 3 shows the volume variation induced by ΔA.

- Since the inclusion is placed at $\vartheta = \vartheta_f$, figure 2 shows that in vesicles characterized by greater spontaneous curvatures the shape modifications gather away from the inclusion.
- An area increase induces a shape perturbation ϱ_1 that does not change sign all along the vesicle (we will find below that this is not the case when the volume is also constrained).
- Figure 3 shows that the volume increase induced by ΔA increases monotonically with ΔA. However, the remarkable increase in ΔV that appears when $\varsigma_0 \simeq 3$ is to be linked with the spontaneous-curvature driven budding transition [24] that is close to occurring. A detailed analysis of the inclusion's influence on this transition can be performed only by studying the nonlinear shape equation (1.3), and will be reported elsewhere [25].

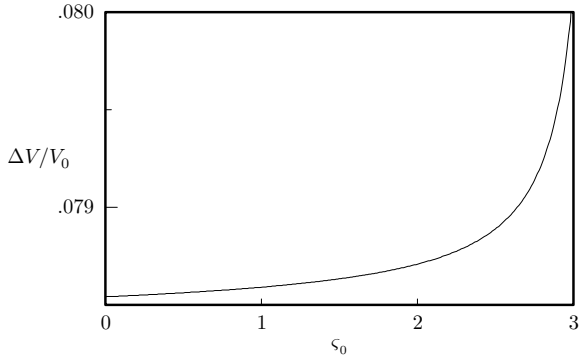

Figure 3. Volume variation induced by a given area variation in a permeable vesicle hosting an inclusion as a function of the reduced spontaneous curvature ς_0. As in figure 2, $\psi_0 = 0.1\pi$ and $\Delta A = 0.05A_0$.

3.1. Small inclusions

By using the asymptotic expansion (A.5), it is possible to show that in the small inclusion limit $a \ll \sqrt{A_0}$, which implies $\psi_0 \ll 1$ by virtue of (2.3), the perturbed vesicle shape becomes independent of ς_0

$$r(\vartheta) = r_0\left(1 + \frac{\Delta A}{A_0}\frac{1+\cos\vartheta}{2}\right) + O\left(\psi_0^2 \lg\psi_0, \left(\frac{\Delta A}{A_0}\right)^2\right). \tag{3.4}$$

Figure 2 shows that when the spontaneous curvature is small, the asymptotic expression (3.4) is more rapidly approached. In fact, if we compute the volume variation associated with the perturbed shape (3.4) we obtain

$$\frac{\Delta V}{V_0} = \frac{3}{2}\frac{\Delta A}{A_0} + O\left(\psi_0^2 \lg\psi_0, \left(\frac{\Delta A}{A_0}\right)^2\right).$$

Figure 3 confirms that the relative volume variation is closer to the small limit prediction $\frac{3}{2}\Delta A/A_0$ when ς_0 is small.

4. Impermeable vesicles

We now focus on the solutions of the differential equation (2.9) that satisfy both area and volume constraints, when these geometrical quantities are close to satisfying the spherical condition (2.4). Leaving aside for the moment the cases $\nu = 0$ and $\nu = 1$ (that turn out to be meaningless in the impermeable case), the solution of (2.9) is of the form (2.12) with the following parameters to be determined: C_1, C_2, C_3, C_4, Λ_0 (i.e. ν, by virtue of (2.11)), and the combination $(\Lambda_1 + \eta_1)$.

4.1. Singular perturbations

The boundary conditions (2.1) and (2.2) may determine the four parameters C_1–C_4. A problem arises when we try to determine ν and $(\Lambda_1 + \eta_1)$ by using the area and volume constraints. In fact, $O(\epsilon)$ of the above constraints reads

$$\int_0^{\vartheta_f} \varrho_1(\vartheta)\sin\vartheta\,\mathrm{d}\vartheta = \frac{\Delta A}{4\pi r_0^2} \qquad \int_0^{\vartheta_f} \varrho_1(\vartheta)\sin\vartheta\,\mathrm{d}\vartheta = \frac{\Delta V}{2\pi r_0^3}. \tag{4.1}$$

It is clearly impossible to satisfy both constraints if

$$\Delta A \neq \frac{2}{r_0}\Delta V.$$

From the analytical point of view, the degeneracy of constraints (4.1) stems from the fact that the first variations of area and volume of a surface are linearly dependent when computed in a spherical shape. In fact, if we perturb any surface with constant mean curvature H (the so-called Delaunay surfaces [26, 27]), the area and volume of the resulting surface satisfy [23]

$$\Delta A = 2H\Delta V.$$

The area and volume constraints become linearly independent only when the second variations come into play. Thus, if we are willing to perturb the assigned area and volume to an arbitrary $O(\epsilon)$, we have to perturb the shape function $r(\vartheta)$ to $O(\sqrt{\epsilon})$, as we shall show next.

We begin by replacing (2.5) by

$$r(\vartheta) = r_0\big(1 + \sqrt{\epsilon}\varrho_{\frac{1}{2}}(\vartheta) + \epsilon\varrho_1(\vartheta) + o(\epsilon)\big). \tag{4.2}$$

The singular perturbation $\varrho_{\frac{1}{2}}$ is of the form (2.12), with Λ_1 and η_1 replaced by their half-order counterparts $\Lambda_{\frac{1}{2}}$ and $\eta_{\frac{1}{2}}$. Correspondingly, the area and enclosed volume of the resulting vesicle shape are given by

$$\begin{aligned} A_0 + \epsilon\Delta A &= 2\pi\int_0^{\vartheta_f} r\sqrt{r^2 + r'^2}\sin\vartheta\,\mathrm{d}\vartheta \\ &= A_0 + 4\pi r_0^2\sqrt{\epsilon}\int_0^{\vartheta_f}\varrho_{\frac{1}{2}}\sin\vartheta\,\mathrm{d}\vartheta + \pi r_0^2\epsilon\int_0^{\vartheta_f}\big(2\varrho_{\frac{1}{2}}^2 + \varrho_{\frac{1}{2}}'^2 + 4\varrho_1\big)\sin\vartheta\,\mathrm{d}\vartheta + o(\epsilon) \end{aligned} \tag{4.3}$$

$$\begin{aligned} V_0 + \epsilon\Delta V &= \frac{2\pi}{3}\int_0^{\vartheta_f} r^3(\vartheta)\sin\vartheta\,\mathrm{d}\vartheta \\ &= V_0 + 2\pi r_0^3\sqrt{\epsilon}\int_0^{\vartheta_f}\varrho_{\frac{1}{2}}\sin\vartheta\,\mathrm{d}\vartheta + \pi r_0^3\epsilon\int_0^{\vartheta_f}\big(2\varrho_{\frac{1}{2}}^2 + 2\varrho_1\big)\sin\vartheta\,\mathrm{d}\vartheta + o(\epsilon). \end{aligned} \tag{4.4}$$

Both (4.3) and (4.4) can now be satisfied, provided the functions $\varrho_{\frac{1}{2}}$ and ϱ_1 are such that

$$\int_0^{\vartheta_f}\varrho_{\frac{1}{2}}(\vartheta)\sin\vartheta\,\mathrm{d}\vartheta = 0 \tag{4.5}$$

$$\int_0^{\vartheta_f}\big[\varrho_{\frac{1}{2}}'^2(\vartheta) - 2\varrho_{\frac{1}{2}}^2(\vartheta)\big]\sin\vartheta\,\mathrm{d}\vartheta = \frac{r_0\Delta A - 2\Delta V}{\pi r_0^3} \tag{4.6}$$

and

$$\int_0^{\vartheta_f}\varrho_1(\vartheta)\sin\vartheta\,\mathrm{d}\vartheta = \frac{\Delta V}{2\pi r_0^3} - \int_0^{\vartheta_f}\varrho_{\frac{1}{2}}^2(\vartheta)\sin\vartheta\,\mathrm{d}\vartheta. \tag{4.7}$$

Equations (4.5) and (4.6) fix $\varrho_{\frac{1}{2}}$, as we will show below; then, equation (4.7) allows us to determine also the next-order correction ϱ_1.

Before entering the detailed analysis of equations (4.5) and (4.6), the above result deserves some remarks:

- Equation (4.2) underlines the most striking effect of the impermeability constraint on the vesicle: an $O(\epsilon)$ perturbation of the assigned geometrical values induces an $O(\sqrt{\epsilon})$ perturbation in the vesicle shape.

- Equation (4.5) is an eigenvalue equation. We have to look for non-trivial (i.e. non-vanishing) perturbations $\varrho_{\frac{1}{2}}$ that satisfy it. It will prove to admit a countable infinity of independent solutions.
- Equation (4.6) is quadratic in $\varrho_{\frac{1}{2}}$. We will thus find two, rather than one, possible perturbed shapes for any non-trivial solution of (4.5). An energy argument will be needed to identify the preferred perturbation among the double-infinity of possible choices at our disposal. Both perturbed shapes arising from (4.6) will deserve notice, since they display two qualitatively different vesicle reactions to the perturbation.
- The quadratic expression in the left-hand side of (4.6) forces the right-hand side combination $(r_0\Delta A - 2\Delta V)$ to assume only non-negative values. This property is not peculiar to vesicle theory: it reflects a classical isoperimetric inequality. In fact, for any closed surface, the ratio A^3/V^2 is bounded from below by the value 36π, which is attained only by a sphere (see, e.g., [28] p 8). Thus, for example, there does not exist a closed surface with the same enclosed volume as a sphere and smaller area.

4.2. Multiplicity of stationary perturbed shapes

The free boundary conditions (2.2) require that the coefficients of the singular Legendre functions of the second kind in (2.12) must be null: $C_2 = C_4 = 0$. Afterwards, the contact conditions (2.1), which are linear in the shape function, supply two relations that connect C_1, C_3 and $\left(\Lambda_{\frac{1}{2}} + \eta_{\frac{1}{2}}\right)$ in (2.12). As a result, the leading perturbation $\varrho_{\frac{1}{2}}$ in (4.2) can be given in the form:

$$\varrho_{\frac{1}{2}}(\vartheta) = C_3[\alpha(\nu, \psi_0) + \beta(\nu, \psi_0)\cos\vartheta + P_\nu(\cos\vartheta)] \tag{4.8}$$

with

$$\alpha(\nu, \psi_0) = -\operatorname{cosec}^2\psi_0(\nu\cos\psi_0 P_{\nu-1}(-\cos\psi_0) + (\sin^2\psi_0 + \nu\cos^2\psi_0)P_\nu(-\cos\psi_0))$$

and

$$\beta(\nu, \psi_0) = -\nu\operatorname{cosec}^2\psi_0(P_{\nu-1}(-\cos\psi_0) + \cos\psi_0 P_\nu(-\cos\psi_0)).$$

In order to determine completely the function $\varrho_{\frac{1}{2}}$, we have to use (4.5) and (4.6) to derive ν and C_3. Any non-trivial solution of (4.5) possesses $C_3 \neq 0$. Thus, we can drop C_3 to obtain an eigenvalue equation in ν, depending only on ψ_0. Figure 4 illustrates the numerical solutions of (4.5). These solutions exhibit the following properties:

- The spontaneous curvature does not enter (4.5). Thus, the stationary shape modifications of an impermeable vesicle do not depend on ς_0, as they did in the permeable case (see (3.1) and figure 2).
- For any $\psi_0 \in \left[0, \frac{\pi}{2}\right]$, there is a countable infinity of values $\nu_k(\psi_0)$ satisfying (4.5).
- For any $\psi_0 \in \left[0, \frac{\pi}{2}\right]$, the solutions $\nu_k(\psi_0)$ are symmetric with respect to $\nu = -\frac{1}{2}$. However, since the symmetric solutions are identical (see (A.1)), we can restrict our attention to solutions with $\nu \geqslant -\frac{1}{2}$.
- When $\psi_0 \ll 1$ (small protein limit), the use of (A.5) allows us to prove that ν_k tends to an integer value for any k:

$$\nu_k(\psi_0) = (k+1) + \frac{k-1}{4}\psi_0^2 + o(\psi_0^2) \qquad \text{for any} \quad k \in \mathbb{N}. \tag{4.9}$$

  The shape function thus approaches a linear combination of Legendre functions of integer order, that is Legendre polynomials. Furthermore, both (4.9) and figure 4 show that only Legendre polynomials of order equal to or greater than 2 come into play, while only

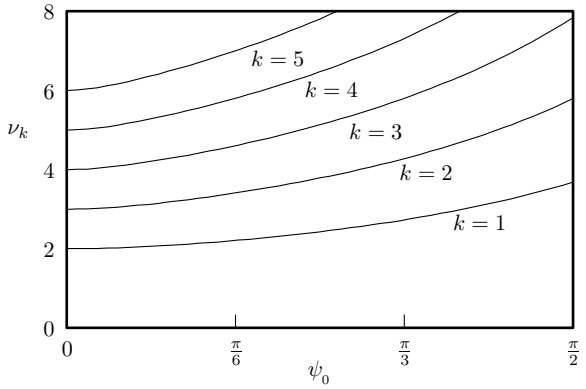

Figure 4. Order ν of the Legendre functions entering the perturbation of an impermeable vesicle shape as a function of the inclusion apex angle ψ_0. The graphs display the smallest five numerical solutions $\{\nu_k, k = 1, \ldots, 5\}$ of equation (4.5).

low-order Legendre polynomials (P_0 and P_1) entered the small-protein limit of permeable vesicles (see (3.4)). This yields more drastic shape modifications in the incompressible case, since Legendre polynomials are more and more oscillating as their order increases. The expansion of the shape function (in the absence of inclusions) in terms of Legendre polynomials was first used in [24].

- For any $k \in \mathbb{N}$, the functions $\nu_k(\psi_0)$ increase monotonically with ψ_0, and do not intersect.
- It is possible to prove by direct inspection that $\nu = 0$ and $\nu = 1$ do not solve (4.5) for any value of ψ_0.

Once we have identified the ν-values that satisfy (4.5), we can insert (4.8) in (4.6) to determine C_3, the only remaining free parameter in the singular perturbation $\varrho_{\frac{1}{2}}$. We stress again that, $\varrho_{\frac{1}{2}}$ being linear in C_3, the latter parameter enters quadratically in (4.6). This fact, on the one hand fixes a sign for the geometrical quantity $(r_0\Delta A - 2\Delta V)$, and on the other hand implies that, for any $k \in \mathbb{N}$ with $\nu = \nu_k(\psi_0)$, there are exactly two values of C_3 (one the opposite of the other) that satisfy (4.6). Thus, for any $k \in \mathbb{N}$, there are two possible perturbed shapes: $r_{k\pm}(\vartheta) = r_0\big(1 \pm \sqrt{\epsilon}\varrho_{\frac{1}{2},k}(\vartheta) + O(\epsilon)\big)$.

Only an energy estimate can help us determine, for any $\psi_0 \in \big[0, \frac{\pi}{2}\big]$, both the value of ν_k and the sign of C_3 that minimize the elastic energy. This will be the aim of the remaining part of this section.

4.3. Energy estimates

4.3.1. Ground state energy. In order to identify which is energetically preferred among the stationary perturbed shapes determined above, we will now compute their elastic energy. When we insert (4.2) in the free-energy functional (1.1), and we make use of (4.5)–(4.7), we obtain

$$\begin{aligned}\mathcal{F}_{k\pm} &= 2\pi\kappa \int_0^{\vartheta_f} (H_{k\pm} - \sigma_0)^2 r_{k\pm}\sqrt{r_{k\pm}^2 + r_{k\pm}'^2}\,\sin\vartheta\,\mathrm{d}\vartheta \\ &= \kappa(\varsigma_0 - 1)^2\frac{A_0}{r_0^2} + \kappa\varsigma_0(\varsigma_0 - 1)\frac{\Delta A}{r_0^2} - \kappa\varsigma_0\frac{r_0\Delta A - 2\Delta V}{r_0^3} + \mathcal{F}_k^{(2)} + o(r_0\Delta A, \Delta V)\end{aligned}$$

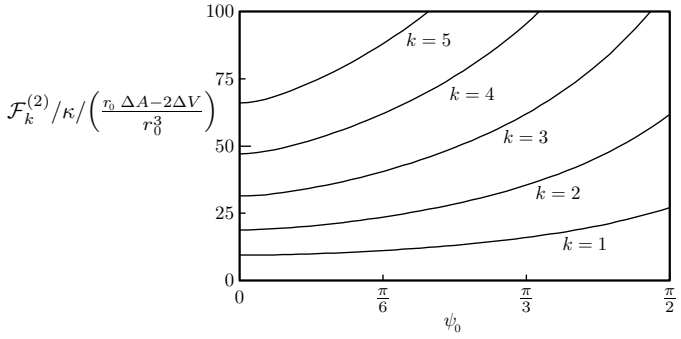

Figure 5. Results of the numerical computation of the integral in (4.10), when $\varrho_{\frac{1}{2},k}$ is given in (4.8), and ν is the kth solution of equation (4.5). The graphs display the results for $k = 1, \ldots, 5$.

where $\mathcal{F}_{k\pm}$ denotes the free energy of the kth solution of equation (4.5), with positive or negative sign for C_3, and

$$\mathcal{F}_k^{(2)} = \frac{\pi}{2}\kappa \int_0^{\vartheta_f} \left[\varrho'^2_{\frac{1}{2},k}(\vartheta)\frac{\cos 2\vartheta}{\sin^2\vartheta} + \varrho''^2_{\frac{1}{2},k}(\vartheta) \right] \sin\vartheta \, \mathrm{d}\vartheta \tag{4.10}$$

is the leading order that may determine k and the sign of C_3. However, $\mathcal{F}_k^{(2)}$ depends quadratically on $\varrho_{\frac{1}{2},k}$, so that the sign of C_3 cancels out from it. Thus, the second-order expansion turns out to be able to identify only the preferred value of ν_k. A further term in the free-energy expansion will be needed to complete the determination of the free-energy absolute minimizer.

Figure 5 shows how $\mathcal{F}_k^{(2)}$ depends on k and ψ_0: the free energy increases when either of these increases. In particular, figure 5 proves that the stable perturbed shape for a quasi-spherical impermeable vesicle corresponds to the solution with the smallest possible order of the Legendre functions. This is not surprising from the physical point of view, since Legendre functions wrinkle when their order increases, and these oscillations increase the elastic energy.

4.3.2. Pear-shaped or stomatocytes? We still have to choose the preferred sign for the parameter C_3. Figure 6 shows the deep, qualitative, differences between permeable (a) and impermeable ((b) and (c)) stationary shapes that arise from the same parameter changes: $\Delta A = \frac{1}{10}A_0$ for all the shapes; ΔV is left free in (a), while it is kept null in (b) and (c). Permeable vesicles modify their enclosed volume in order to keep an almost-spherical shape. In contrast, impermeable vesicles move towards pear-shaped or stomatocyte-like equilibrium shapes [29], depending on the sign of C_3.

In order to compare the free energies of pear-shaped and stomatocyte-like vesicles, we need to push our free-energy expansion further. The next order depends on the third power of $\varrho_{\frac{1}{2}}$ and its derivatives: it is $O(r_0\Delta A, \Delta V)^{3/2}$. By making use of the constraint requirements (4.5)–(4.7), it is possible to obtain

$$\mathcal{F}_{(\mathrm{ps,st})} = \kappa(\varsigma_0 - 1)^2\frac{A_0}{r_0^2} + \kappa\varsigma_0(\varsigma_0 - 1)\frac{\Delta A}{r_0^2} - \kappa\varsigma_0\frac{r_0\Delta A - 2\Delta V}{r_0^3} + \mathcal{F}^{(2)} + \mathcal{F}^{(3)}_{(\mathrm{ps,st})} + o(r_0\Delta A, \Delta V)^{3/2}$$

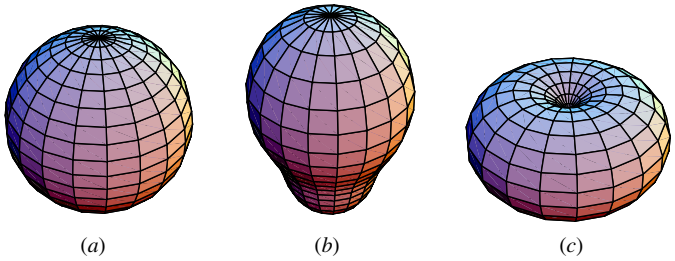

Figure 6. Perturbed shapes for a vesicle embedding an inclusion of negligible size ($\psi_0 \ll 1$) when a 10% increase in the vesicle area is imposed (with respect to the value leading to a spherical shape): (*a*) shows the equilibrium shape of a permeable vesicle, which is allowed to adapt its enclosed volume, (*b*) and (*c*) refer to an impermeable vesicle when the positive or negative sign for the parameter C_3 is chosen when solving equation (4.5). The inclusion (not visible here) sits in the bottom end of the vesicle.

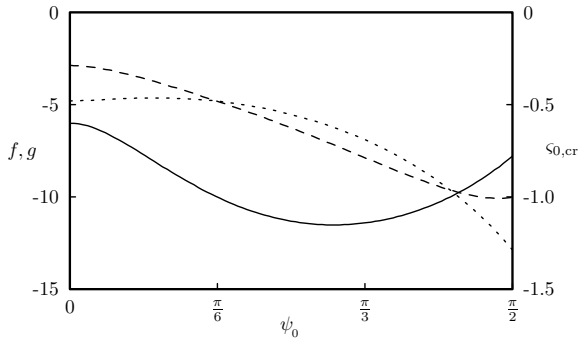

Figure 7. Plots of the functions f (dashed), g (dotted line), introduced in (4.11), and the critical spontaneous curvature $\varsigma_{0,\mathrm{cr}}$ (continuous line), defined in (4.12), all as functions of the apex angle.

where all the terms up to $\mathcal{F}^{(2)}$ do not depend on the pear shaped versus stomatocyte choice, and

$$\mathcal{F}^{(3)}_{(\mathrm{ps,st})} = \pm\left(\frac{r_0\Delta A - 2\Delta V}{r_0^3}\right)^{\frac{3}{2}} (f(\psi_0) + \varsigma_0 g(\psi_0)). \tag{4.11}$$

In (4.11), the plus sign corresponds to the pear-shaped vesicle, the minus sign describes a stomatocyte and ς_0 denotes as usual the reduced spontaneous curvature. Plots of the functions f and g (whose explicit expressions can be found in appendix B, equations (B.2)–(B.3)) are shown in figure 7. Both f and g are negative for all values of ψ_0. Thus, for any positive value of the spontaneous curvature, the pear-shaped vesicle is the absolute minimizer of the free energy, whereas the stomatocyte represents only a relative minimum. A transition between the two stationary shapes can be observed only when negative spontaneous curvatures are induced; more precisely, the stomatocyte-like phase is preferred if

$$\varsigma_0 < -\frac{f(\psi_0)}{g(\psi_0)} =: \varsigma_{0,\mathrm{cr}}(\psi_0). \tag{4.12}$$

Figure 7 also shows how the critical value of the reduced spontaneous curvature depends on the apex angle. In particular, $-\frac{6}{5} < \varsigma_{0,\mathrm{cr}}(\psi_0) \leqslant -\frac{3}{5}$ for all values of ψ_0.

5. Concluding remarks

In this paper we have analysed how the impermeability constraint may induce singular stationary vesicle shapes, and how the embedding of an inclusion may vary the vesicle topology, promoting pear-shaped geometries that anticipate critical phenomena such as budding or vesiculation [30, 31].

Our analysis has been based on the linearization of the shape equation close to a spherical shape. This approximation does not allow us to approach the aforementioned transitions, but in turn yields analytical results which prove that the vesicle reaction to a variation of the external parameters may not be analytical. In section 4 we have shown that an $O(\epsilon)$ relative variation in the vesicle area may induce either an $O(\epsilon)$ or an $O(\sqrt{\epsilon})$ relative variation in the shape function, depending on the permeability properties of the vesicle and the aqueous solution that surrounds it.

The present analytical study is being currently completed by a numerical study [25], which detects how the presence of an embedded inclusion modifies the phase diagrams describing the vesicle topology, and under which conditions it anticipates budding phenomena.

Acknowledgments

This work was made possible by the post-doctoral fellowship 'Mathematical Models for Fluid Membranes', supported by the Mathematics Department of the *Politecnico di Milano*. Some of the analytical computations and figures presented in this paper were performed with the aid of Mathematica® 4.1, licence: L4596-4499.

Appendix A. Properties of Legendre functions

The Legendre functions of the first and second kind (respectively denoted as $P_\nu(s)$ and $Q_\nu(s)$) are the solutions of the linear differential equation

$$(1-s^2)y''(s) - 2sy'(s) + \nu(\nu+1)y(s) = 0.$$

The Legendre functions of the first kind are regular when $s \to 1^-$ (with $P_\nu(1) = 1$), while the Legendre functions of the second kind are singular close to both $s = \pm 1$. The properties we use in this paper are the following (see [32], sections 8.2 and 8.5).

For any $\nu \in \mathbb{R}$ and $s \in [-1, 1]$

$$P_{-\frac{1}{2}-\nu}(s) = P_{-\frac{1}{2}+\nu}(s) \tag{A.1}$$

$$P_{\nu+1}(s) = \frac{2\nu+1}{\nu+1} s P_\nu(s) - \frac{\nu}{\nu+1} P_{\nu-1}(s) \qquad (\nu \neq -1) \tag{A.2}$$

$$(1-s^2)P'_\nu(s) = \nu P_{\nu-1}(s) - \nu s P_\nu(s). \tag{A.3}$$

Equations (A.2) and (A.3) imply

$$\int P_\nu(\cos\vartheta)\sin\vartheta \,\mathrm{d}\vartheta = -\int P_\nu(s)\,\mathrm{d}s = \frac{P_{\nu-1}(\cos\vartheta) - \cos\vartheta\, P_\nu(\cos\vartheta)}{\nu+1} \qquad (\nu \neq -1). \tag{A.4}$$

For any $\nu \in \mathbb{R}^+\backslash\mathbb{N}$, the Legendre functions of the first kind admit the following asymptotic expansion:

$$P_\nu(-1+\epsilon) = -\frac{\lg(\epsilon/2) + 2\gamma + \Psi(-\nu) + \Psi(\nu+1)}{\Gamma(-\nu)\Gamma(\nu+1)} + O(\epsilon \lg \epsilon) \qquad \text{as} \quad \epsilon \to 0^+ \tag{A.5}$$

where Γ, Ψ and γ respectively denote the Euler gamma function, the digamma function and Euler's constant.

Appendix B. Third order expansion of the free energy

The derivation of the third-order term in the free-energy expansion requires a third-order expansion of the shape function. Thus, (4.2) has to be replaced by

$$r(\vartheta) = r_0\big(1 + \sqrt{\epsilon}\varrho_{\frac{1}{2}}(\vartheta) + \epsilon\varrho_1(\vartheta) + \epsilon^{\frac{3}{2}}\varrho_{\frac{3}{2}}(\vartheta) + o\big(\epsilon^{\frac{3}{2}}\big)\big).$$

However, the higher-order terms ϱ_1 and $\varrho_{\frac{3}{2}}$ turn out to enter the free-energy expansion only through combinations that can be related to integrals of $\varrho_{\frac{1}{2}}$ and its derivatives by making use of the area and volume constraints, as already happens in the second-order expansion (see (4.7)). More precisely, the third-order expansion of the constraints yields

$$\int_0^{\vartheta_f} \varrho_{\frac{3}{2}}(\vartheta)\sin\vartheta\,\mathrm{d}\vartheta + 2\int_0^{\vartheta_f} \varrho_1(\vartheta)\varrho_{\frac{1}{2}}(\vartheta)\sin\vartheta\,\mathrm{d}\vartheta = -\frac{1}{3}\int_0^{\vartheta_f} \varrho_{\frac{1}{2}}^3(\vartheta)\sin\vartheta\,\mathrm{d}\vartheta. \tag{B.1}$$

By using (B.1) it is long but straightforward to prove that

$$\mathcal{F}_{(\mathrm{ps,st})} = \kappa(\varsigma_0 - 1)^2\frac{A_0}{r_0^2} + \kappa\varsigma_0(\varsigma_0 - 1)\frac{\Delta A}{r_0^2} - \kappa\varsigma_0\frac{r_0\Delta A - 2\Delta V}{r_0^3} + \mathcal{F}^{(2)} + \mathcal{F}^{(3)} + o(r_0\Delta A, \Delta V)^{3/2}$$

with

$$\mathcal{F}^{(3)}_{(\mathrm{ps,st})} = F(\psi_0) + \varsigma_0 G(\psi_0)$$

where

$$F(\psi_0) = 2\pi\int_0^{\vartheta_f}\left[\frac{\nu_k(1+\nu_k)}{3}\varrho_{\frac{1}{2}}^3 - \frac{\cos 2\vartheta}{1-\cos 2\vartheta}\varrho_{\frac{1}{2}}\varrho_{\frac{1}{2}}'^2 + \frac{\cot\vartheta}{6}\varrho_{\frac{1}{2}}'^3 - \frac{1}{2}\varrho_{\frac{1}{2}}\varrho_{\frac{1}{2}}'^2\right]\sin\vartheta\,\mathrm{d}\vartheta$$

$$G(\psi_0) = 2\pi\int_0^{\vartheta_f}\left[\varrho_{\frac{1}{2}}\varrho_{\frac{1}{2}}'^2 - \frac{2}{3}\varrho_{\frac{1}{2}}^3 + \frac{1}{3}\varrho_{\frac{1}{2}}'^3\cot\vartheta\right]\sin\vartheta\,\mathrm{d}\vartheta.$$

The functions f, g introduced in (4.11) are related to F, G through

$$f(\psi_0) = F(\psi_0)\,\mathrm{sgn}(C_3)\left(\frac{r_0\Delta A - 2\Delta V}{r_0^3}\right)^{-\frac{3}{2}} \tag{B.2}$$

$$g(\psi_0) = G(\psi_0)\,\mathrm{sgn}(C_3)\left(\frac{r_0\Delta A - 2\Delta V}{r_0^3}\right)^{-\frac{3}{2}}. \tag{B.3}$$

References

[1] Schekman R and Orci L 1996 Coat proteins and vesicle budding *Science* **271** 1526–33

[2] Huttner W B and Zimmerberg J 2001 Implications of lipid microdomains for membrane curvature, budding and fission *Curr. Opin. Cell Biol.* **13** 478–84

[3] Huttner W B and Schmidt A A 2002 Membrane curvature: a case of endofeelin'... *Trends Cell Biol.* **12** 155–8

[4] Biscari P and Rosso R 2001 Inclusions embedded in lipid membranes *J. Phys. A: Math. Gen.* **34** 439–59

[5] Koltover I, Rädler J O and Safinya C R 1999 Membrane mediated attraction and ordered aggregation of colloidal particles bound to giant phospholipid vesicles *Phys. Rev. Lett.* **82** 1991–4

[6] Biscari P and Bisi F 2002 Membrane-mediated interactions of rod-like inclusions *Eur. Phys. J.* **7** 381–6

[7] Biscari P, Bisi F and Rosso R 2002 Curvature effects on membrane-mediated interactions of inclusions *J. Math. Biol.* **45** 37–56

[8] Goulian M, Bruinsma R and Pincus P 1993 Long-range forces in heterogeneous fluid membranes *Europhys. Lett.* **22** 145–50

[9] Golestanian R, Goulian M and Kardar M 1996 Fluctuation-induced interactions between rods on membranes and interfaces *Europhys. Lett.* **33** 241–5

[10] Weikl T R, Kozlov M M and Helfrich W 1998 Interaction of conical membrane inclusions: effect of lateral tension *Phys. Rev.* E **57** 6988–95

[11] Dommersnes P G, Fournier J-B and Galatola P 1998 Long-range elastic forces between membrane inclusions in spherical vesicles *Europhys. Lett.* **42** 233–8
[12] Seifert U 1991 Vesicles of toroidal topology *Phys. Rev. Lett.* **66** 2404–7
[13] Jülicher F and Lipowsky R 1996 Shape transformations of vesicles with intramembrane domains *Phys. Rev.* E **53** 2670–83
[14] Dan N, Pincus P and Safran S A 1993 Membrane-induced interactions between inclusions *Langmuir* **9** 2768–71
[15] Dan N and Safran S A 1998 Effect of lipid characteristics on the structure of transmembrane proteins *Biophys. J.* **75** 1410–4
[16] Park J-M and Lubensky T C 1996 Interactions between membrane inclusions on fluctuating membranes *J. Phys.* I **6** 1217–35
[17] Dommersnes P G and Fournier J-B 1999 Casimir and mean-field interactions between membrane inclusions subject to external torques *Europhys. Lett.* **42** 256–61
[18] Dommersnes P G and Fournier J-B 2002 The many-body problem for anisotropic membrane inclusions and the self-assembly of 'saddle' defects into an 'egg carton' *Biophys. J.* **83** 2898–905
[19] Nielsen C and Andersen O S 2000 Inclusion-induced bilayer deformations: effects of monolayer equilibrium curvature *Biophys. J.* **79** 2583–604
[20] Helfrich W 1973 Elastic properties of lipid bilayers: theory and possible experiments *Z. Naturforsch.* **28** 693–703
[21] Deuling H J and Helfrich W 1976 The curvature elasticity of fluid membranes: a catalogue of vesicle shapes *J. Phys.* **37** 1335–45
[22] Zhong-can O-Y and Helfrich W 1987 Instability and deformation of a spherical vesicle by pressure *Phys. Rev. Lett.* **59** 2486–8
[23] Zhong-can O-Y and Helfrich W 1989 Bending energy of vesicle membranes: General expressions for the first, second, and third variation of the shape energy and applications to spheres and cylinders *Phys. Rev. A* **39** 5280–88
[24] Wiese W and Helfrich W 1990 Theory of vesicle budding *J. Phys.: Condens. Matter* **2** 329–32
[25] Biscari P and Napoli G in preparation
[26] Delaunay C 1841 Sur la surface de révolution, dont la corbure moyenne est constante *J. Math. Pures Appl.* **6** 309–15
[27] Naito H, Okuda M and Zhong-Can O-Y 1995 New solutions to the Helfrich variation problem for the shapes of lipid bilayer vesicles: beyond Delaunay's surfaces *Phys. Rev. Lett.* **74** 4345–8
[28] Pólya G and Szegö G 1951 *Isoperimetric Inequalities in Mathematical Physics* (Princeton, NJ: Princeton University Press)
[29] Seifert U, Berndl K and Lipowsky R 1991 Shape transformations of vesicles: phase diagram for spontaneous-curvature and bilayer-coupling models *Phys. Rev.* A **44** 1182–202
[30] Miao L, Fourcade B, Rao M, Wortis M and Zia R K P 1991 Equilibrium budding and vesiculation in the curvature model of fluid lipid vesicles *Phys. Rev.* A **43** 6843–56
[31] Fourcade B, Miao L, Rao M, Wortis M and Zia R K P 1994 Scaling analysis of narrow necks in curvature models of fluid lipid-bilayers vesicles *Phys. Rev.* E **49** 5276–86
[32] Abramowitz M and Stegun I A 1972 *Handbook of Mathematical Functions* 10th printing